# Realization and Characterization of Porous Gold for Increased Protein Coverage on Acoustic Sensors

Kristien Bonroy,*,† Jean-Michel Friedt,† Filip Frederix,† Wim Laureyn,† Steven Langerock,‡ Andrew Campitelli,† Margit Sára,§ Gustaaf Borghs,† Bruno Goddeeris,|| and Paul Declerck⊥

*IMEC, MCP-BIO, Kapeldreef 75, B-3001 Leuven, Belgium, Coördination Chemistry, KULeuven, Celestijnenlaan 200G, B-3001 Leuven, Belgium, Center for Ultrastructure Research and Ludwig Boltzmann-Institute for Molecular Nanotechnology, A-1180 Vienna, Austria, Laboratory for Physiology and Immunology of Domestic Animals, KULeuven, Kasteelpark Arenberg 30, B-3001 Leuven, Belgium, and Laboratory for Pharmaceutical Biology and Phytopharmacology, KULeuven, Van Evenstraat 4, B-3000 Leuven, Belgium*

**Immunosensors show great potential for the direct detection of biological molecules. The sensitivity of these affinity-based biosensors is dictated by the amount of receptor molecules immobilized on the sensor surface. An enlargement of the sensor area would allow for an increase of the binding capacity, hence a larger amount of immobilized receptor molecules. To this end, we use electrochemically deposited "gold black" as a porous sensor surface for the immobilization of proteins. In this paper, we have analyzed the different parameters that define the electrochemical growth of porous gold, starting from flat gold surfaces, using different characterization techniques. Applied potentials of −0.5 V versus a reference electrode were found to constitute the most adequate conditions to grow porous gold surfaces. Using cyclic voltammetry, a 16 times increase of the surface area was observed under these electrochemical deposition conditions. In addition, we have assessed the immobilization degree of alkanethiols and of proteins on these different porous surfaces. The optimized deposition conditions for realizing porous gold substrates lead to a 11.4-fold increase of thiol adsorption and a 3.3-fold increase of protein adsorption, using the quartz crystal microbalance (QCM-D) as a biological transducer system. Hence, it follows that the high specific area of the porous gold can amplify the final sensitivity of the original flat surface device.**

In recent years, there has been an increasing need for the detection of low concentrations of (bio)chemical substances with a low molecular weight such as residues, hormones, and drugs.[1−3] Biosensors can provide a rapid and convenient alternative to conventional analytical methods for monitoring these substances in various fields such as medicine, environmental monitoring, fermentation processes, and food processing.[4−6] In general, a biosensor consists of two parts, i.e., a transducer and an affinity-based interface, which leads to the variation of a physical quantity when the analyte of interest binds to the sensor system. The affinity biosensor interface of immunosensors consists of antibodies, which are attached to the transducer surface, preferably via a linking layer. A number of methods has been applied for the immobilization of receptor biomolecules[7−9] on transducer surfaces, i.e., adsorption at a solid surface,[10] covalent attachment to silanes[11] and thiols,[12−16] and entrapment in polymer matrixes[17,18] and membranes.[19] In previous research, the use of self-assembled monolayers (SAMs) of silanes and thiols on, respectively, flat oxide or gold surfaces showed several advantages concerning specificity

* To whom correspondence should be addressed. Phone: +32-16-281050. Fax: +32-16-281097. E-mail: Kristien.bonroy@imec.be.

† IMEC.

‡ Coördination Chemistry, KULeuven.

§ Center for Ultrastructure Research and Ludwig Boltzmann-Institute for Molecular Nanotechnology.

|| Laboratory for Physiology and Immunology of Domestic Animals, KULeuven.

⊥ Laboratory for Pharmaceutical Biology and Phytopharmacology, KULeuven.

(1) Bilitewski, U. *Anal. Chem.* **2000**, *72* (21), 692A−701A.
(2) Pemberton, R. M.; Hart, J. P.; Mottram, T. T. *Biosens. Bioelectron.* **2001**, *16*, 715−723.
(3) Nath, N.; Eldefrawi, M.; Wright, J.; Darwin, D.; Huestis, M. *J. Anal. Toxicol.* **1999**, *23*, 460−467.
(4) Mulchandani, A.; Rogers, K. R. *Enzyme and Microbial Biosensors: Techniques and Protocols*; Humana: Totowa, NJ, 1998.
(5) Ramsay, G. *Commercial Biosensors: Applications to Clinical Bioprocess and Environmental Samples*; John Wiley & Sons: London, 1998.
(6) Nikolelis, D.; Krull, U.; Wang, J.; Mascini, M. *Biosensors for Direct Monitoring of Environmental Polluants in Field*; Kluwer Academic: London, 1998.
(7) Rogers, K. R. *Mol. Biotechnol.* **2000**, *14*, 109−129.
(8) Cass, T.; Ligler, F.S. *Immobilized Biomolecules in Analysis: A Practical Approach*; Oxford University Press: New York, 1998.
(9) Hermanson, G. T.; Mallia, A.K. *Immobilized Affinity Ligand Techniques*; Academic Press: London, 1992.
(10) Castner, D. G.; Ratner, B. D. *Surf. Sci.* **2000**, *500*, 28−60.
(11) Laureyn, W. Physicochemical study on the use of silanes for the realization of oxide-based biosensor interfaces. Ph.D. Thesis, K.U. L., Leuven, Belgium, 2002.
(12) D'Souza, S. F. *Appl. Biochem. Biotechnol.* **2001**, *96*, 225−238.
(13) Frederix, F.; Bonroy, K.; Laureyn, W.; Reekmans, G.; Campitelli, A.; Dehaen, W.; Maes, G. *Langmuir* **2003**, *19* (10), 4351−4357.
(14) Ferretti, S.; Paynter, S.; Russell, D. A.; Sapsford, K. E.; Richardson D. J. *Trends Anal. Chem.* **2000**, *19* (9), 530−540.
(15) Spinke, J.; Liley, M.; Schmitt, F.-J.; Guder, H.-J.; Angermaier, L.; Knollet, W. *J. Chem. Phys.* **1993**, *99* (9), 7012−7019.
(16) Göpel, W.; Heiduschka, P. *Biosens. Bioelectron.* **1995**, *10*, 853−883.
(17) Huang, N.-P.; Vönös, J.; De Paul, S. M.; Textor, M.; Spencer, N. D. *Langmuir* **2002**, *18*, 220−230.
(18) Cosnier, S. *Biosens. Bioelectron.* **1999**, *14*, 443−456.
(19) Cooper, M. A. *Nat. Rev. Drug Discovery* **2002**, *1*, 515−528.

10.1021/ac049893u CCC: $27.50 © xxxx American Chemical Society
Published on Web 00/00/0000



PAGE EST: 7.5

and reproducibility for final biosensor applications.[11,13,20−23] However, the main disadvantage of this approach is the two-dimensional aspect of these surfaces compared to three-dimensional surfaces. The latter allows for a higher immobilization degree of bioreceptor molecules per unit area, presumably resulting in a higher biosensor signal. Different approaches have been described to increase the amount of receptor molecules on transducer surfaces, i.e., three-dimensional linking layers such as dextran layers,[24,25] dendrimers layers,[26−28] and porous substrates such as porous silicon[29−31] and porous gold.[32−34] Although dextran layers are known to be one of the best nonfouling surfaces,[35] they show a long-term drift[36] and a large nonspecific protein binding in certain applications.[13,26] Three-dimensional layers of dendrimers also exhibit high nonspecific signals and a low reproducibility, due to their highly charged nature and complex immobilization protocol.[26] Even though porous silicon has been shown to adsorb more proteins compared to porous gold,[37] the latter might be more suitable for biosensor applications because of its higher stability in a variety of conditions (i.e., biochemical buffer solutions) compared to porous silicon.[32] In addition, porous gold can be combined with the well-characterized and optimized SAMs of thiols, which are often used as linking layers for immunosensors. Furthermore, porous gold surfaces are compatible with the state-of-the-art transducer systems for direct detection, e.g., surface plasmon resonance and quartz crystal microbalance (QCM).[34] Because of its inertness, high surface area, and excellent electrical conductivity, porous gold can also be useful for other applications such as catalysis or ultracapacitor research.[38] This paper reports on the systematic approach to growing various porous gold surfaces. More specifically, we describe the optimization of the electrochemical deposition of porous gold on flat gold crystals by varying the applied potentials and the deposition time, using the QCM-D technique for on-line characterization. The resulting gold surfaces are characterized using scanning electron microscopy (SEM), cyclic voltammetry (CV), and contact angle geometry (CA). In addition, the adsorption of alkanethiols and surface layer (S-layer) proteins, which respectively recrystallize into monolayers and monomolecular protein lattices and do not stack as multiple layer structures even at high concentrations,[39,40] were used as a model system to evaluate the increased molecule and protein coverage on the different porous gold surfaces using QCM-D technique.

## EXPERIMENTAL SECTION

**Materials.** Hydrogen tetrachloroaurate hydrate, tris(hydroxymethyl)aminoethane (Tris), and lead(II) acetate were purchased from Sigma-Aldrich. Calcium chloride and ultrapure ethanol were obtained from Riedel-DeHaën. Sulfuric acid was received from VWR. 2-(2-(2-(6-Mercaptohexyloxy)ethoxy)ethoxyl)ethanol (HS-$(CH_2)_6(OCH_2CH_2)_3OH$, or 6-PEO-thiol) was synthesized as described in Frederix et al.[13] Diiodomethane was purchased from Acros, while octadecanethiol ($CH_3$-thiol) was from TCI Europe. The 14-mm blank plano-plano QCM AT-cut quartz crystals were purchased from Chintele Quartz Technology Co. Ltd. (Zhejiang, China). S-layers (protein SbpA from *Bacillus sphaericus* CCM 2177) were kindly supplied by the research group of Prof. U. B. Sleytr (Center for Ultrastructure Research and Ludwich Bolzman Institute for Molecular Nanotechnology, Vienna, Austria).

**Substrate Preparation.** The Ti/Au (5/50 nm) electrodes were deposited on bare AT-cut quartz crystals by electron beam evaporation using a mechanical mask. The sensing electrode consists of a 12-mm-diameter disk that covers one side of the crystal, while the opposite side is patterned with a keyhole-shaped electrode made of a central 5-mm-diameter disk and a 3-mm-long, 1-mm-wide lead to the edge of the crystal (total area, 23 $mm^2$). Before porous gold deposition, the flat gold crystals were cleaned for 15 min using a homemade UV/$O_3$ device with an ozone producing Mercury Grid lamp (BHK Inc.) and rinsed with ethanol to remove organic contamination.[41] The electrochemical deposition of gold was performed using a three-electrode system with an Ag/AgCl reference electrode and a Pt counter electrode according to a procedure described by Imamura et al.[33] The liquid cell (o-ring inner area, 32 $mm^2$) was described in Friedt et al.[42] and allows for simultaneously QCM-D measurements (Q-sense AB, Göteberg, Sweden) while depositing the porous gold by a potentiostatic setup (Gamry PC3-300 potentiostat and Framework software). In this combined setup, the sensing surface of the QCM crystals can be simultaneously used as the electrochemical working electrode (WE) because the frequencies of the electrical signals generated by the two techniques differ widely.[42] The solution used to grow porous structures contained 0.08 M hydrogen tetrachloroaurate and 0.004 M lead acetate. Potentials between −0.4 and −0.6 V versus a Ag/AgCl reference electrode and different deposition times between 10 and 50 s were applied. The potentiostat registers current changes as a function of time with a sampling rate of 100


(20) Williams, R. A.; Blanch, H. W. *Biosens. Bioelectron.* **1994**, *9*, 159−167.
(21) Mirsky, V. M.; Riepl, M.; Wolfbeis, O. S. *Biosens. Bioelectron.* **1997**, *12*, 977−989.
(22) Raman Suri, C.; Mishra, G. C. *Biosens. Bioelectron.* **1996**, *11*, 1199−1205.
(23) Maupas, H.; Saby, C.; Martelet, C.; Jaffrezic-Renault, N.; Soldatkin, A. P.; Charles, M.; Delair, T.; Mandrand, B. *J. Electroanal. Chem.* **1996**, *406*, 53−58.
(24) Löfas, S.; Johnsson, B. *J. Chem. Soc., Chem. Commun.* **1990**, *21*, 1526−1528.
(25) Johnsson, B.; Löfås, S.; Lindquist, G. *Anal. Biochem.* **1991**, *198*, 268−277.
(26) Frederix, F. The use of self-assembly for the realization of immunosensor interfaces and systems. Ph.D. thesis; K. U. L., Leuven, Belgium, 2004.
(27) Yoon, H. C.; Hong, M.-Y.; Kim, H.-S. *Langmuir* **2001**, *17*, 1234−1239.
(28) Hong, M.-Y.; Yoon, H. C.; Kim, H.-S. *Langmuir* **2003**, *19*, 416−421.
(29) Lin, V. S.-Y.; Motesharei, K.; Dancil, K.-P. S.; Sailor, M. J.; Ghadiri, M. R. *Science* **1997**, *278*, 840−843.
(30) Thust, M.; Schöning, M. J.; Schroth, P.; Malkoc, Ü.; Dicker, C. I.; Steffen, A.; Kordos, P.; Lüth, H. *J. Mol. Catal. B: Enzym.* **1999**, *7*, 77−83.
(31) Karlsson, L. M.; Tengvall, T.; Lundström, I.; Arwin, H. J. *Colloid Interface Sci.* **2003**, *266*, 40−47.
(32) Van Noort, D.; Mandenius, C.-F. *Biosens. Bioelectron.* **2000**, *15*, 203−209.
(33) Imamura, M.; Haruyama, T.; Kobatake, E.; Ikariyama, Y.; Aizawa, M. *Sens. Actuators, B* **1995**, *24*, 113−116.
(34) Van Noort, D.; Rani, R.; Mandenius, C.-F. *Mikrochim. Acta* **2001**, *136*, 49−53.
(35) Myska, D. G. *J. Mol. Recognit.* **1999**, *12*, 197−284.
(36) Storri, S.; Santoni, T.; Minunni, M.; Mascini, M. *Biosens. Bioelectron.* **1997**, *13*, 347−357.
(37) Van Noort, D.; Welin-Klintström, S.; Arwin, H.; Zangooie, S.; Lundström, I.; Mandenius, C.-F. *Biosens. Bioelectron.* **1998**, *3-4*, 439−449.
(38) Cortie, M.; van der Lingen, E.; Valenzuela, S.; Martin, D. Properties and potential applications of meso-porous gold. Presented at Gold, Vancouver, 28th Sept−1st Oct, 2003.
(39) Weygand, M.; Wetzer, W.; Pum, D.; Sleytr, U. B.; Cuvillier, N.; Kjaer, K.; Howes, P. B.; Lösche, M. *Biophys. J.* **1999**, *76*, 458−468.
(40) Pum, D.; Neubauer, A.; Györvary, E.; Sára, M.; Sleytr, U. B. *Nanotechnology* **2000**, *11*, 100−107.
(41) Vig, J. R. *J. Vac. Sci. Technol., A* **1985**, *3* (3), 1027−1034.
(42) Friedt, J.-M.; Choi, K. H.; Frederix, F.; Campitelli, A. *J. Electrochem. Soc.* **2003**, *150*, H229−234.

Table 1. QCM-D and Potentiostatic Measurements during the Deposition of Different Porous Gold Samples[a]

| potential (V) | deposition time (s) | $\Delta D$ ($\times 10^{-6}$)[b] | $\Delta f_3/3$ (Hz) | $\Delta f_5/5$ (Hz) | $\Delta f_7/7$ (Hz) | $\Delta f_n/n$ (Hz) | Rel $\sigma$ ($f_n/n$) (%) | $\Delta f_3/\sqrt{3}$ (Hz) | $\Delta f_5/\sqrt{5}$ (Hz) | $\Delta f_7/\sqrt{7}$ (Hz) | Rel $\sigma$ ($f_n/\sqrt{n}$) (%) | $M_I$ ($\mu$g/cm$^2$) | $M_{QCM}$ ($\mu$g/cm$^2$) | % ratio $M_{QCM}$ vs $M_I$ |
|---|---|---|---|---|---|---|---|---|---|---|---|---|---|---|
| −0.5 | 10 | 17 | 5043 | 5047 | 5050 | 5047 | 0.1 | 8734 | 11285 | 13362 | 20.8 | 84 | 101 | 21 |
| −0.5 | 12 | 45 | 6467 | 6509 | 6490 | 6489 | 0.3 | 11201 | 14555 | 17171 | 20.9 | 103 | 130 | 27 |
| −0.5 | 15 | 81 | 7208 | 7280 | 7277 | 7255 | 0.6 | 12485 | 16279 | 19253 | 21.2 | 121 | 146 | 20 |
| −0.5 | 20 | 96 | 10428 | 10327 | 10334 | 10363 | 0.5 | 17932 | 23053 | 27289 | 20.6 | 184 | 208 | 13 |
| −0.4 | 15 | 3 | 7156 | 7227 | 7299 | 7227 | 1.0 | 12394 | 16160 | 19311 | 21.7 | 122 | 145 | 19 |
| −0.4 | 20 | 2 | 8969 | 9104 | 9202 | 9092 | 1.3 | 15535 | 20358 | 24345 | 22.0 | 155 | 183 | 18 |
| −0.4 | 30 | 3 | 12914 | 13223 | 13632 | 13256 | 2.7 | 22368 | 29567 | 36067 | 23.4 | 235 | 266 | 14 |
| −0.4 | 40 | 6 | 16915 | 17557 | 18151 | 17541 | 3.5 | 29297 | 39259 | 48022 | 24.1 | 310 | 353 | 14 |

[a] Dissipation shifts ($\Delta D$) and frequency shifts ($\Delta f_n$ with $n = 3, 5, 7$) normalized by $n$ or by $\sqrt{n}$ for different porous gold samples. The relative standard deviations (Rel $\sigma$) between the different modes are given for both normalizations. Mass estimation of metal deposited on the QCM sensing electrode as calculated from the total charges transferred during the potentiostatic measurements ($M_I$) and from the frequency shifts ($\Delta f_n/n$) obtained during the QCM-D ($M_{QCM}$) measurements. [b] Average of dissipation shifts for three overtones ($\Delta D_3$, $\Delta D_5$, $\Delta D_7$).

samples/s, while the QCM-D instrument monitors in real time the frequency and dissipation changes.

**Surface Characterization.** The porous gold surfaces were characterized using SEM and CA to obtain qualitative information about the roughness of the realized gold surfaces. A JEOL 5600 LV (HV mode) instrument was used to acquire the SEM images. CA measurements were performed on 1-$\mu$L sessile drops of ultrapure water or diiodomethane, using an OCA 20 system from Dataphysics using SCA 20 software. CV was used to get quantitative information about the increase of the sensor area. The CV measurements were performed in 0.5 M $H_2SO_4$ using a scan speed of 100 mV/s.

**Thiol and Protein Adsorption.** Prior to use, the resulting porous gold surfaces were thoroughly rinsed with water and ethanol and dried under a stream of nitrogen. Subsequently, the crystals were cleaned with UV/$O_3$ for 15 min, again rinsed with ethanol, and dried under a stream of nitrogen before being mounted in the liquid cell. The adsorption of alkanethiols and proteins was monitored using QCM-D, for thiols in combination with a new generation Q-Sense liquid cell (QAFFC302) with solvent resistant Viton tubing, and for proteins in combination with the original first generation Q-Sense liquid cell (o-ring area, 100 mm$^2$). The octadecanethiol was adsorbed from a 1 mM ethanol solution. The S-layer proteins were adsorbed from a solution of 100 $\mu$g/mL in 0.5 mM Tris and 10 mM $CaCl_2$ buffer (pH ~8). After a short sensor signal stabilization in ethanol or S-layer buffer, the thiol or protein solution was left on the sensor surface for, respectively, 20 min and 1 h until an adsorption plateau was reached. Subsequently, the surface was flushed with ethanol or buffer to remove loosely bound thiol molecules or proteins. The shift before and after adsorption of the molecules was measured in ethanol for the thiol molecules and in S-layer buffer for the S-layer proteins.

## RESULTS AND DISCUSSION

**Electrochemical Deposition and in Situ Characterization of Porous Gold.** The evolution of the frequency and damping of the QCM crystals was simultaneously recorded for the third, fifth, and seventh overtones (fundamental mode, ~4.7 MHz), together with the current resulting from the applied potential difference during the deposition of porous gold. The different porous surfaces were obtained by varying the applied potential (−0.4, −0.5, or −0.6 V versus Ag/AgCl reference electrode) and the deposition time (from 10 to 50 s) (Table 1). A typical QCM-D curve is shown in Figure 1, which displays the frequency and dissipation evolution for the seventh overtone during electrochemical deposition under an applied potential of −0.5 V. After a stable signal of 60 s, the gold deposition is initiated, resulting in a change in frequency and dissipation (Figure 1). The QCM frequency shift provides an estimate of the total mass of metal deposited on the whole sensing electrode, while the QCM dissipation rises when viscous interactions with the surrounding liquid increase.[42,43] Not all depositions could be monitored on-line with the QCM-D technique. Some of the deposition conditions lead to a loss of the oscillation at the highest overtones because of the fast dissipation increase due to the large amount of deposited mass, due to the interaction of the deposited layer with the surrounding liquid, or due to both. Electrochemical deposition of porous gold using a potential of −0.6 V did not allow for full on-line measurements, as after only 12-s deposition time the quartz crystal stopped oscillating. Potentials

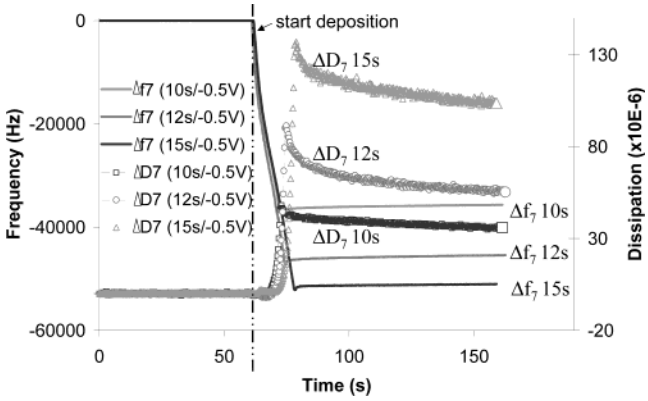


Figure 1. Typical QCM-D curves observed while depositing porous gold. The left axis shows the frequency shifts for the seventh overtone ($\Delta f_7$); the right axis shows the dissipation changes ($\Delta D_7$), during electrochemical deposition of porous gold under an applied potential of −0.5V with varying deposition times. A delay of the dissipation increase, compared to the frequency shift, indicated by the dotted line, is observed. Subsequently, the dissipation reaches a maximum, followed by a slow decrease to a stable dissipation signal.

(43) Rodahl, M.; Hook, F.; Fredriksson, C.; Keller, C. A.; Krozer, A.; Brzezinski, P.; Voinova, M.; Kasemo, B. *Faraday Discuss.* **1997**, *107*, 229−246.

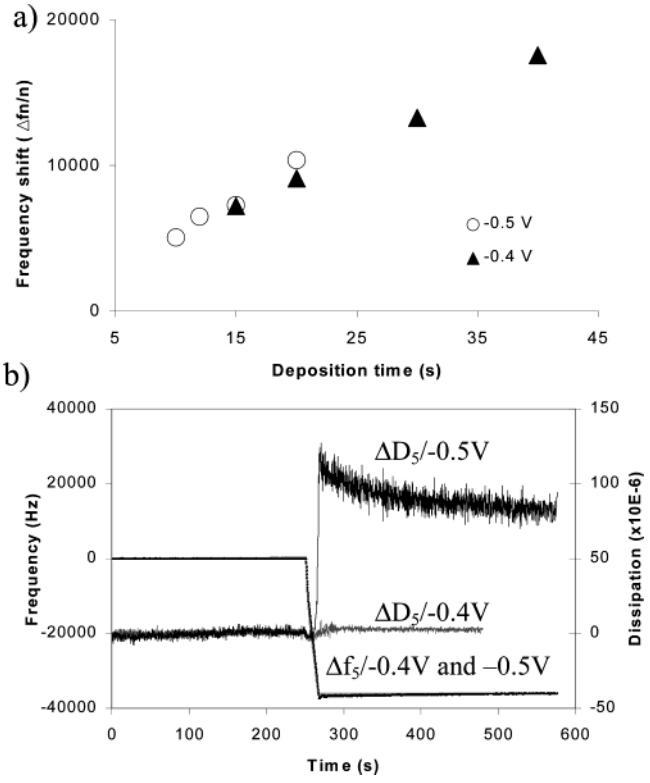


Figure 2. (a) QCM-D frequency shifts for different deposition times of porous gold under an applied potential of −0.4 and −0.5 V. (b) Comparison of the QCM-D curves for different deposition potentials (−0.5 versus −0.4 V). The left axis shows $\Delta f_5$, and the right axis shows $\Delta D_5$, both during 15 s of deposition of porous gold under an applied potential of −0.4 and −0.5 V.

of −0.4 and −0.5 V resulted in more stable measurements. A potential of −0.5 V allowed for on-line measurements until 20 s, while for a potential of −0.4 V, the crystal kept oscillating at all overtones even after 40 s of deposition time. During on-line measurements of the mass deposition, the frequency and dissipation shifts were recorded. The frequency shift was found to be linear with the deposition time (Figure 2a) but rather independent of the applied potential. The latter conclusion is supported by the observation that, for similar deposition times, no difference in frequency shift is observed if the potential is varied between −0.4 and −0.5 V (Figure 2b). The dissipation shifts, on the contrary, showed an increase with the applied potential (Figure 2b). This indicates that a lower deposition potential (i.e., −0.4 V) gives rise to surfaces that interact less with the surrounding liquid compared to higher potentials such as −0.5 V. Following this observation and the fact that the crystals realized with higher potential stopped oscillating, the structure of the gold deposited using higher potentials is expected to be more rough. This was confirmed using SEM imaging (Figure 3). As a result, the extent of the QCM damping could be used as an on-line indicator for the final surface roughness. While monitoring the dissipation shifts of the surfaces with increased roughness, an intriguing behavior was observed. The samples prepared at a potential of −0.5 V showed a dissipation that started rising after a delay of a few seconds compared to the frequency increase (Figure 1). Subsequently, the dissipation reached a maximum, followed by a slow decrease until a stable dissipation signal was obtained. The frequency shift on the contrary decreased immediately upon application of the negative potential. The SEM images revealed only spots of gold particles on the original gold substrates during the first 10 s (Figure 3a), while for longer deposition times dendritic structures are realized (Figure 3b,c). It is clear that the increase in dissipation occurred during the formation of these dendritic structures. The slow decrease in the dissipation, after the plateau was reached, was attributed to the morphological relaxation of the gold layer, as previously reported by Schumacher et al.[44]

The QCM curves for the different deposition conditions were compared. For a rigid mass deposition, the frequency shift is expected to be proportional to the overtone. The normalized frequency shifts of the overtones ($\Delta f_n/n$ with $n = 3$, 5, and 7) were indeed found to overlap, which is illustrated by the small relative standard deviation given in Table 1. A scaling by $\Delta f_n/n^{1/2}$, as would be expected for a predominantly viscous interaction, gives less satisfactory results. This is shown in Table 1 by the high relative standard deviation between $\Delta f_n/n^{1/2}$ values obtained for the different modes. These observations allow us to assume that a predominantly rigid mass is deposited,[42,45] which only acts as an increased thickness of the added gold layer on the resonator. As reported in the literature,[42] this rigid mass assumption is expected for electrochemical depositions, which results in smooth layers, as seen at the −0.4 V plating conditions. Interestingly, for depositions at −0.5 V, where a large increase in the damping is recorded, the same curve overlap of the $\Delta f_n/n$ shifts is also observed. This indicates that the rigid interaction due to a very large deposited mass is still predominant over the viscous interactions. From these considerations, we conclude that the conversion of the frequency shift to an added mass using the Sauerbrey relationship is valid. The mass sensitivity of the QCM is given by the Sauerbrey equation[46] (valid for rigid mass) applied to the $n$th overtone

$$\Delta f_n = \frac{-n2f_1^2}{A\sqrt{\rho\mu}}\Delta m$$

where $\rho = 2.684$ g cm$^{-3}$ is the density of quartz, $\mu = 2.947 \times 1011$ g cm$^{-1}$ s$^{-2}$ is the shear modulus of AT-cut quartz, $A$ is the macroscopic sensing area, $n$ the overtone number, and $f_1$ is the fundamental resonance frequency (4.7 MHz). The mass deposited on the QCM can be deduced by multiplying the normalized observed frequency shift of the $n$th overtone $\Delta f_n/n$ by a proportionality factor of 20.1 ng Hz$^{-1}$ cm$^{-2}$. From the calculated mass, a maximum thickness of the grown gold layers can be deduced. Assuming flat gold layers were grown, and taking into account the density of gold (19.3 g/cm$^3$), the minimum thickness of the deposited gold layer was calculated to be between 52.3 and 180 nm (depending on the deposition conditions).

We compare the estimated mass of metal deposited on the QCM sensing electrode as deduced from the normalized frequency shift with the total charge transferred as measured by the potentiostatic measurement (Table 1). The number of charges transferred to the system by the electrochemical setup is numeri-

(44) Schumacher, R.; Gordon, J.G.; Melroy, O. *J. Electroanal. Chem.* **1987**, *216*, 127−135.
(45) Friedt, J.-M.; Francis, L.; Choi, K.-H.; Campitelli, A. *J. Vac. Sci. Technol., A* **2003**, *21*, 1500−1505.
(46) Sauerbrey, G. Z. *Phys.* **1959**, *155*, 206−212.

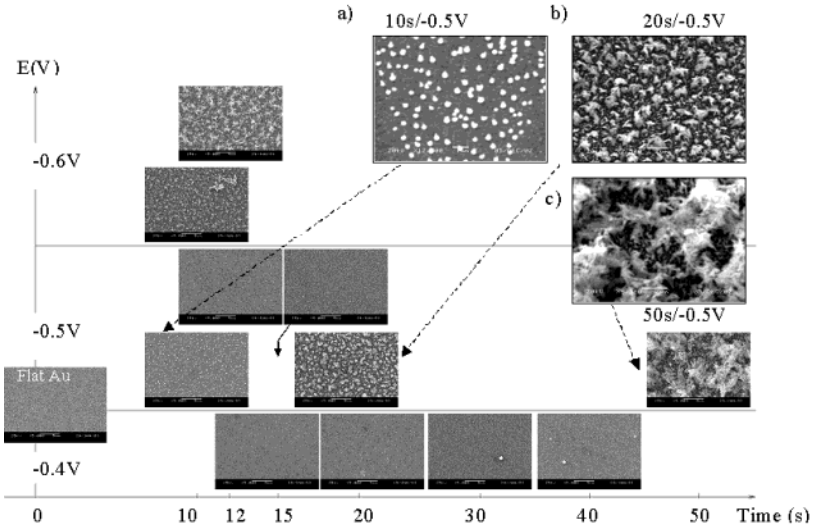


Figure 3. SEM images of the porous gold samples for different deposition times (10−50 s) and potentials (−0.4/−0.5/−0.6 V) used during electrodeposition (×5000; scale 5 $\mu$m). Zooms of gold samples (a) 10 s/−0.5 V (×12000; scale 1 $\mu$m), (b) 20 s/−0.5 V (×7500; scale 2$\mu$m), and (c) 50 s/−0.5 V (×9500; scale 2 $\mu$m) are given.

cally integrated and leads to a deposited mass of

$$M_{\text{deposited}} = \frac{M_{\text{Au}} \Sigma_j I_j \, \delta t}{Z_{\text{ion}} F}$$

where $F$ is the Faraday constant ($F$ = 96440 C), $\Sigma_j I_j$ is the numerical integration of the measured current, $\delta t$ is the time interval between two current measurements, $Z_{\text{ion}}$ is the valence of the metallic ion (i.e., 3 for $Au^{3+} \rightarrow$ Au), $M_{\text{deposited}}$ is the mass of metal deposited on the WE, and $M_{\text{Au}}$ is the molar weight of the metal deposited on the surface (196.97 g/mol for gold). As shown in Table 1, the mass calculated from the electrochemical charges is systematically less (13−26%) than the mass calculated from the experimentally observed QCM frequency shift, assuming a rigid mass model. This means that the sensitivity of the QCM as calculated from the Sauerbrey equation is overestimated. Similar discrepancies were reported previously.[42,47] We attribute this mass discrepancy, according to Schumacher et al.,[47] to the increase of the surface roughness and thus to the trapped water interacting rigidly with the surface.

**Ex Situ Characterization of Porous Gold.** Besides the on-line characterization using the QCM-D technique and the resulting current flow during deposition, the gold was also characterized ex situ after deposition. SEM was used for a qualitative characterization of the different surfaces (Figure 3). When analyzing the SEM images, the surfaces formed using an applied potential of −0.6 and −0.5 V display rougher structures compared to those deposited using −0.4 V. When comparing the samples of −0.6 to −0.5 V, we observe that these higher potentials result in porous structures after only 10 s, while at a potential of −0.5 V, a longer time is needed to grow dendritic structures. These results are in good agreement with the assessment following the on-line QCM measurements. A significant difference in behavior of the damping during deposition of the samples (−0.4 and −0.5 V) did hint already toward a difference in porosity. The SEM images (Figure 3) confirm that the increase of the damping found for the −0.5 V samples was a good indication for their roughness.

Contact angle measurements were performed to obtain additional qualitative information of the different surfaces. According to different models, the surface wettability is dependent on the surface porosity.[48,49] The model of Wenzel[50] proposed the following dependence of the contact angle to the surface roughness:

$$\cos \theta_r = r \cos \theta_{\text{true}}$$

with $r$ the ratio of the actual area to the projected area, $\theta_r$ the measured contact angle, and $\theta_{\text{true}}$ the expected contact angle. This formula predicts that contact angles of >90° for a flat surface will result in an increased contact angle upon increased surface porosity, while contact angles of <90° will decrease upon increased surface roughness.[51] To assess whether the model applies for our surfaces, we immobilized a 6-PEO-thiol SAM and a hydrophobic $CH_3$-thiol SAM on the cleaned porous gold surfaces and measured the static contact angle with water and diiodomethane (Figure 4). A 6-PEO-thiol SAM on a flat gold surface resulted in a static water contact angle of 31° ± 1°, as predicted by Frederix et al.[26] For the 15, 30, and 40 s of the −0.4 V sample series, contact angles of, respectively, 32° ± 5°, 28° ± 1°, and 29° ± 6° were found for this hydrophilic thiol. These contact angles showed no significant variation for the different deposition times. Most of the samples realized at −0.6 and −0.5 V resulted in contact angle values below 5° (denoted 0°). Only the 10 s/-0.5 V sample showed a measurable contact angle of 24° ± 3°. For the hydrophobic $CH_3$-thiol, the water contact angle on a flat gold substrate was 105° ± 4°. The contact angles of the porous gold

(47) Schumacher, R.; Borges, G.; Kanazawa, K. K. *Surf. Sci.* **1985**, *163*, L621−L626.
(48) Adamson, A.W. *Physical Chemistry of Surfaces*; John Wiley and Sons: New York, 1990, 385.
(49) Extrand, C. W. *Langmuir* **2002**, *18*, 7991−7999.
(50) Wenzel, R. N. *J. Phys. Colloid Chem.* **1949**, *53*, 1466−1467.
(51) De Gennes, P.-G.; Brochard-Wyart, F.; Quéré, D. *Gouttes, bulles, perles et ondes*; Belin: Paris, 2002; p 192.

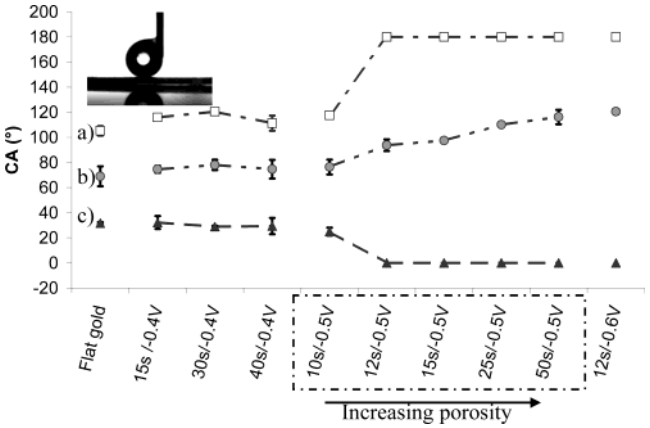


Figure 4. CA measurements for different porous gold surfaces coated with $CH_3$-thiol or PEO-thiol: (a) CA obtained on $CH_3$-thiol using water (squares) or (b) diiodomethane (dots) as a solvent; (c) CA on PEO-thiol on different surfaces using water as a solvent (triangle). The samples in the box on the *x*-axis are ordered as a function of their roughness. The inset shows a picture of a drop of water dispensed via a syringe on a rough surface coated with a hydrophobic thiol.

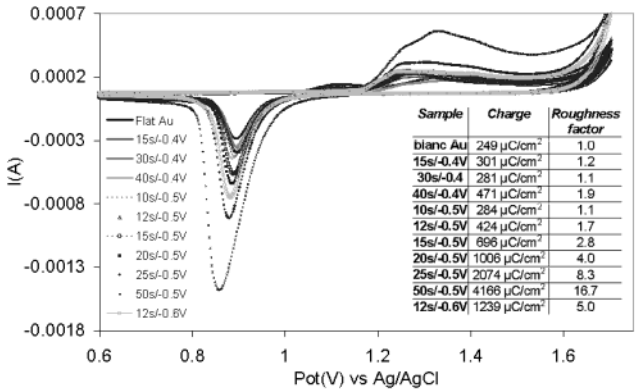


Figure 5. Determination of the surface roughness of the gold samples using cyclic voltammetry in 0.5 M $H_2SO_4$. The integration of the gold oxide reduction peak (~0.85 V) gives an estimate of the actual area of the porous surfaces. The charges per surface area under the cathodic peak and the roughness factor for the different gold surfaces are given in the table.

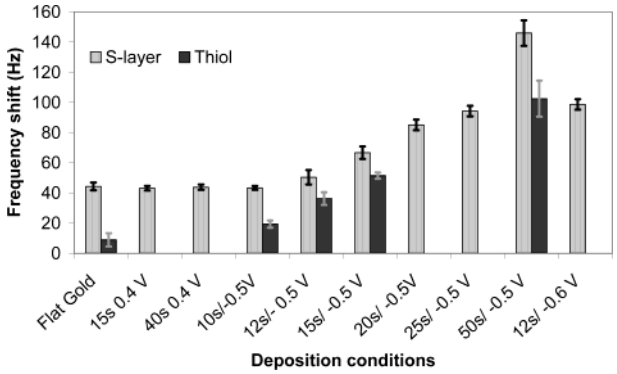


Figure 6. QCM-D frequency shifts ($\Delta f_n/n$), due to thiol and protein adsorptions, showing an increase of the adsorption as a function of the gold roughness.

samples were again only measurable for the 10 s/−0.5 V sample and for the −0.4 V samples. All other samples showed a round drop (CA ~180°) lying on the surface. Following the model of Wenzel, we can conclude from these observations that more porous surfaces are only formed under −0.5 and −0.6 V conditions, while for the −0.4 V smoother surfaces are realized. Because these two surface functionalizations did not allow for a relative qualification of the porosity, contact angle measurements were performed on the hydrophobic thiol SAM with diiodomethane as a solvent, instead of ultrapure water. A similar contact angle value was observed for the flat gold as for the nonporous layers. For the samples grown using −0.5 V, an increasing contact angle is measured with an increasing deposition time (Figure 4). This is in good agreement with the increasing porosity, as observed using SEM (Figure 3). Therefore, this approach can be used to qualitatively compare the roughness of the different gold samples.

Finally, CV was used to estimate the geometrical surface area of the porous gold surfaces. This method is based on the electrochemically induced deposition of an oxygen monolayer on the electrode surface ($Au_2O_3$) and the measurement of the charge corresponding to this monolayer. The area under the cathodic peak on the voltammogram is proportional to the real area of the gold surface and is therefore an indication for the surface roughness.[52−54] The roughness factor can be calculated by the ratio of the area under the cathodic peak of the different porous samples compared to the area obtained for the flat gold sample. Figure 5 shows the CV curves obtained for the different porous samples. The porous gold samples obtained for mild deposition conditions (i.e., −0.4 V and 10 s/−0.5 V) all exhibited similar voltammograms, while samples grown under −0.5 V conditions showed a clear increase corresponding to the electrochemical deposition times. The calculated charge under the cathodic peak varies between 249 $\mu C/cm^2$ for flat gold and 4166 $\mu C/cm^2$ for the most porous sample, obtained after 50 s of deposition at −0.5 V. This indicates a 16 times increase of the surface area, which already shows the potential of this approach to increase the amount of receptor molecules on the surface.

**Thiol and S-Layer Protein Adsorption.** After the realization of the porous gold surfaces, their ability to immobilize alkanethiols and proteins was assessed. To this end, the adsorption of thiol molecules and S-layer proteins was monitored on-line by means of QCM-D instrumentation. The evolution of the frequency and the damping of the QCM crystals were recorded for the first, third, fifth, and seventh overtones. Although some of the porous QCM crystals stopped oscillating at their highest overtones during deposition, they still showed a resonant frequency (for at least one mode) during the adsorption experiments. This is probably due to the larger diameter of the O-ring of the Q-sense liquid cell used for the adsorption experiments compared to the one used in the liquid cell during porous gold deposition.

Frequency shifts were recorded during the adsorption of the octadecanethiol on the different porous surfaces. For the flat initial gold surface, the frequency shift of $\Delta f_n/n$ was ~8 Hz (Figure 6). For more porous surfaces, the frequency shift for thiol adsorption increased with the surface roughness. Figure 6 shows a 11.4 times increase of the signal due to adsorption of thiol molecules with increasing porosity of the gold surfaces.

(52) Bard, A. J. *Electroanalytical Chemistry. A Series of Advances*; Marcel Dekker: New York, 1976; Vol. 9.
(53) Hoogvliet, J. C.; Dijksma, M.; Kamp, B.; van Bennekom, W. P. *Anal. Chem.* **2000**, *72*, 2016−2021.
(54) Trasatti, S.; Petrii, O. A. *Pure Appl. Chem.* **1991**, *63* (5), 711−734.

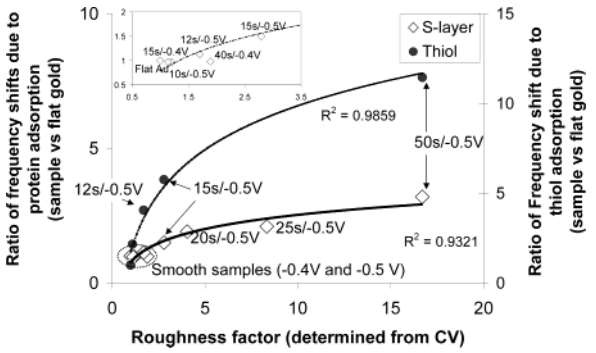


Figure 7. Comparison between the roughness factor determined by cyclic voltammetry (*x*-axis) and the ratio of the frequency shift on the different porous samples and the frequency shift observed on flat gold during thiol adsorption (right *y*-axis) and protein adsorption (left *y*-axis). A linear trend can be seen for the smooth samples, while for the more porous samples a nonlinear trend can be observed. The trend line is added for visual interpretation. The inset shows the comparison of the roughness factor determined by cyclic voltammetry (*x*-axis) and the ratio of the frequency shift on the smooth samples and the frequency shift observed on flat gold during protein adsorption (*y*-axis).

Frequency shifts were also recorded during the adsorption of S-layer protein SbpA on the different porous surfaces. For the flat surfaces, such as the initial gold film, the −0.4 V samples and the 10 s/−0.5 V sample, no significant differences between the frequency shifts are observed and the $\Delta f_n/n$ values were ~43 Hz (Figure 6). For more porous surfaces, the frequency shift for protein adsorption increased with the surface roughness. Figure 6 shows a 3.3 times increase of the signal due to adsorption of S-layers with increasing porosity of the gold surfaces.

When comparing the QCM-D frequency curves during molecule adsorption for the different modes, a good overlap of the normalized frequency of the overtones ($\Delta f_n/n$ with $n = 3$, 5, and 7) can be observed (data not shown), which justifies the rigid mass model. Using the Sauerbrey equation, we estimate a mass load of 160 ± 20 ng/cm² for the octadecanethiol and a mass load of 890 ± 50 ng/cm² for the S-layer proteins on a flat gold crystal, while, respectively, 2240 ± 20 and 2930 ± 170 ng/cm² were found for the most porous sample. The increases of the thiol adsorption (11.4 times) and the protein adsorption (3.3 times) for the more porous surfaces are low compared to that of the area increases observed during the cyclic voltammetry experiments (16 times). There is also a large difference in relative frequency changes observed during the adsorption of the thiols and the proteins on the different surfaces. This observation is explained by the size difference between the thiol molecules and the S-layer proteins. The size of a thiol molecule is ±2 nm, while one morphological unit of S-layer proteins (4 subunits of 127 kDa) occupies a surface area of 13.1 nm × 13.1 nm.[55] Figure 7 plots the roughness factor determined with CV versus the increase of the frequency shift observed during molecule adsorption (compared to flat gold). For the smooth samples (such as 12 s, 15 s and 20 s/−0.5 V, 15 s/−0.4 V, and 40 s/−0.4 V), the increase of adsorption shows a linear behavior with the roughness factor, while the porous samples do not show the expected mass increase resulting in a nonlinear trend

(55) Ilk, N.; Kosma, P.; Puchberger, M.; Egelseer, E. M.; Mayer, H. F.; Sleytr, U. B.; Sára, M. *J. Bacteriol.* **1999**, *18*, 7643−7646.

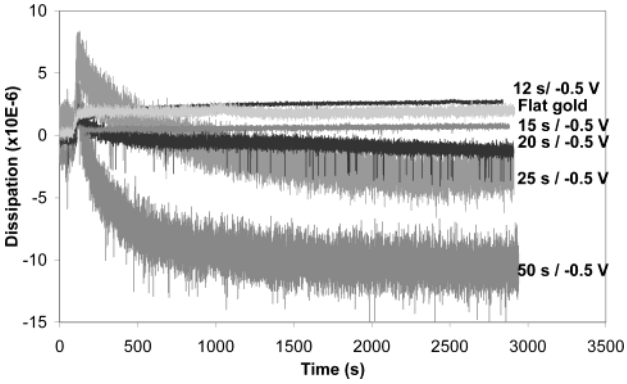


Figure 8. QCM-D dissipation during adsorption of S-layer proteins on different porous gold surfaces. Notice the difference in scale of the dissipation compared to Figure 1.

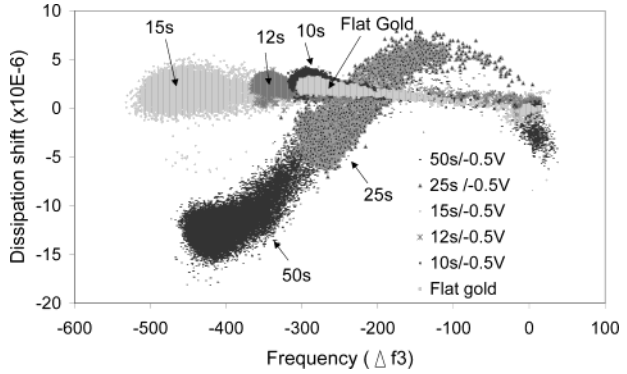


Figure 9. $\Delta D3$ versus $\Delta f3$ plot for different porous surfaces. Different slopes observed in the curves indicate different events occurring on the surface.

line. The latter is probably due to a limited diffusion of the thiol molecules and the proteins in the lower regions of the dentritic structures,[31] leading to lower adsorption values than the ones expected from the cyclic voltammetry data.

As stated above, viscoelastic properties of the adlayers can be estimated by monitoring the dissipation factor or damping. For most of the samples, the dissipation shows a small or even no increase during protein adsorption measurements (Figure 8). This indicates that almost no extra viscous interactions are introduced in this additional measurement step. Since S-layers are assumed to recrystallize into highly monomolecular protein lattices, the water content is assumed to be small and therefore no large viscosity changes are expected.[56] For the more porous samples, such as 20 s, 25 s, 50 s/−0.5 V, and 12 s/−0.6 V, a decrease in the dissipation is observed (Figure 8), which indicates a decrease in the viscosity. In general, the dissipation factor increases with increasing adsorbed mass, since proteins are soft materials.[57] In addition to the evolution of the dissipation, a $\Delta D_3$ versus $\Delta f_3$ plot for the different samples shows a clear difference for the flat and the porous samples (Figure 9). For the flat samples, only one slope is present, indicating the formation of the protein monolayer. The absence of a second slope in $\Delta D_3$ versus $\Delta f_3$ confirms that the formation of a second protein layer is not present. On the $\Delta D_3$

(56) Friedt, J.-M.; Francis, L.; Reekmans, G.; De Palma, R.; Campitelli, A.; Sleytr, U. B. *J. Appl. Phys.*, in press.
(57) Marxer, C. G.; Coen, M. C.; Schlapbach L. J. *Colloids Interface Sci.* **2003**, *261*, 2003, 291−298.

versus $\Delta f_3$ curves for the more rough samples two slopes can be distinguished (Figure 9). The first upward slope indicates the adsorption event of the proteins on the surfaces, while the second downward slope indicates a rigidification of the adlayer. The latter observation can be explained by a diffusion of the proteins in the pores, followed by the replacement of the water trapped in the cavities of the porous surfaces by the proteins, resulting in a lower viscous interaction with the surrounding media.

## CONCLUSION

In this paper, we report on the electrochemical deposition of various porous gold surfaces in order to artificially increase the sensor area, with applications toward biosensors. More specifically, we describe the optimization of the parameters influencing the electrochemical deposition of porous gold by varying the applied potentials and the deposition times. QCM-D was applied to enable the on-line characterization of these porous gold depositions. A potential of −0.5 V versus Ag/AgCl was found to be the most adequate, giving rise to different porous gold morphologies with increasing deposition times. The final surface roughness is determined by the dissipation shift in the on-line QCM-D experiments. Contact angle, cyclic voltammetry, and scanning electron microscopy measurements were used as ex situ characterization tools for the different gold surfaces. The optimized deposition conditions for realizing porous gold substrates lead to a 11.4-fold increase of thiol molecules adsorption and a 3.3-fold increase of protein adsorption using QCM-D as a biological transducer system. Therefore, porous gold allows increasing the amount of immobilized protein, hence the final biosensor signal. In future research, porous gold will be applied in real immunosensing experiments with antibody/antigen systems in combination with optimized thiol SAM chemistry. Furthermore, porous gold might also be useful for other types of sensors such as optical or electrochemical sensors or for other applications where superhydrophobic surface characteristics are of importance.

## ACKNOWLEDGMENT

The authors thank the research group of Prof. U. B. Sleytr of the Center for Ultrastructure Research and Ludwich Bolzman Institute for Molecular Nanotechnology of Vienna for their kind gift of the S-layer protein. We also thank Kang-Hoon Choi from IMEC for performing SEM measurements. Professor L. Heerman of the KULeuven is acknowledged for the useful discussion, and the IWT (Instituut voor de Aanmoediging van Innovatie door Wetenschap en Technologie in Vlaanderen) is gratefully acknowledged for its financial support.

## SUPPORTING INFORMATION AVAILABLE

Graph showing the cyclic voltammetry curves obtained for repetitive cycles on the most porous sample using deposition conditions of −0.5 V/50 s. This material is available free of charge via the Internet at http://pubs.acs.org.

Received for review January 16, 2004. Accepted May 19, 2004.

AC049893U